© M. Horskyi, PhD in physics and mathematics science, Associate professor, K. Felde, PhD in physics and mathematics science, Associate professor, K. Zenkova, Doctor of physics and mathematics of science, Professor, V. Morfliuk-Shchur, PhD in technical science, Assistant, O. Dubolazov, Doctor of physics and mathematics of science, Professor, L. Slotska, PhD in technical science, Associate professor, O. Yatsko, PhD in physics and mathematics science, Associate professor, O. Halochkin, PhD in physics and mathematics science, Associate professor, M. Kovalchuk, PhD in physics and mathematics science, Associate professor, Chernivtsi National University, Chernivtsi, Ukraine, O. Shostachuk, PhD in technical science, Associate professor, Igor Sikorskyi KPI, Kyiv, Ukraine

LASER METROLOGY OF ANISOTROPIC POLYMER LAYERS STRUCTURE OF MATERIALS FOR PACKAGING INDUSTRY

We have proposed the use of a laser-polarimetric method, as more informative in terms of displaying optically inhomogeneous structures by using spatially coherent filtering.

Keywords: applied programming; polymers; publishing; digital and graphic information; packaging materials; materials science.

Introduction

The main idea of using filtering [1–5] is that the spatial-frequency nature of the Fourier images of the polymer layer laser image of the packaging material is different in its large-scale and small-scale components.

Thus, spatial-frequency filtering can isolate both low-frequency and high-frequency components, which are then transformed into the corresponding filtered images of multiscale anisotropic structures using the inverse Fourier transform [6, 7].

The article provides a substantiation of the principles of consistent spatial-frequency polarization-correlation selection for investigation the linear and circular phase anisotropy of polymeric materials.

Method

The analysis of the conversion of laser radiation by polycrystalline grids of various polymeric spheres is based on the following model representations [8–10]:

— the polymer is considered as a two-component isotropic-anisotropic (birefringent) structure;

— the optical-anisotropic component of the polymer is formed by linearly birefringent whiskers, which introduce different spatial-frequency phase modulation between the orthogonal components of the laser beam amplitude.

If a low-pass filter R or a high-pass filter R^{-1} is placed in the central part of the Fourier plane

$$R(\Delta v, \Delta \mu) = \begin{cases} 1 \rightarrow \eta^* \in \Delta \eta; \mu^* \in \Delta \mu; \\ 0 \rightarrow \eta^* \notin \Delta \eta; \mu^* \notin \Delta \mu, \end{cases} \quad (1)$$

$$R^{-1}(\Delta \eta, \Delta \mu) = \begin{cases} 1 \rightarrow \eta^* \notin \Delta \eta; \mu^* \notin \Delta \mu; \\ 0 \rightarrow \eta^* \in \Delta \eta; \mu^* \in \Delta \mu \end{cases}, \quad (2)$$

after it is possible to distinguish the next spatial-frequency structures of the Fourier spectra of the azimuth and ellipticity distributions of the boundary field, that formed either mainly by the effects of linear $\hat{U}(\kappa, \gamma, \eta, \mu)$ or circular $\dot{U}(\psi, \eta, \mu)$ anisotropy

$$\begin{cases} \hat{U}(\kappa, \gamma, \eta, \mu) = \\ = R(\Delta \eta, \Delta \mu) U(\eta, \mu); \\ \dot{U}(\psi, \eta, \mu) = \\ = R^{-1}(\Delta \eta, \Delta \mu) U(\eta, \mu). \end{cases} \quad (3)$$

The corresponding distributions of complex amplitudes in the image plane of the polymer layer can be restored using the inverse FFT

$$\begin{bmatrix} \hat{E}_x(\kappa, \gamma, x, y) \\ \dot{E}_x(\psi, x, y) \end{bmatrix} \text{ and } \begin{bmatrix} \hat{E}_y(\kappa, \gamma, x, y) \\ \dot{E}_y(\psi, x, y) \end{bmatrix}.$$

$$\begin{cases} \hat{E}_x(\kappa, \gamma, x, y) = \\ = \dfrac{1}{i\lambda f} \displaystyle\int_{-\infty}^{+\infty}\int R(\Delta \eta, \Delta \mu) \cdot \\ \cdot \hat{U}_x(\eta, \mu) \exp \cdot \\ \cdot \left[i2\pi(x\eta + y\mu) \right] d\eta d\mu \\ \dot{E}_x(\psi, x, y) = \\ = \dfrac{1}{i\lambda f} \displaystyle\int_{-\infty}^{+\infty}\int R^{-1}(\Delta \eta, \Delta \mu) \cdot \\ \cdot \dot{U}_x(\eta, \mu) \exp \cdot \\ \cdot \left[i2\pi(x\eta + y\mu) \right] d\eta d\mu \end{cases} \quad (4)$$

$$\begin{cases} \hat{E}_y(\kappa, \gamma, x, y) = \\ = \dfrac{1}{i\lambda f} \displaystyle\int_{-\infty}^{+\infty}\int R(\Delta \eta, \Delta \mu) \cdot \\ \cdot \hat{U}_y(\eta, \mu) \exp \cdot \\ \cdot \left[i2\pi(x\eta + y\mu) \right] d\eta d\mu. \\ \dot{E}_y(\psi, x, y) = \\ = \dfrac{1}{i\lambda f} \displaystyle\int_{-\infty}^{+\infty}\int R^{-1}(\Delta \eta, \Delta \mu) \cdot \\ \cdot \dot{U}_y(\eta, \mu) \exp \cdot \\ \cdot \left[i2\pi(x\eta + y\mu) \right] d\eta d\mu \end{cases} \quad (5)$$
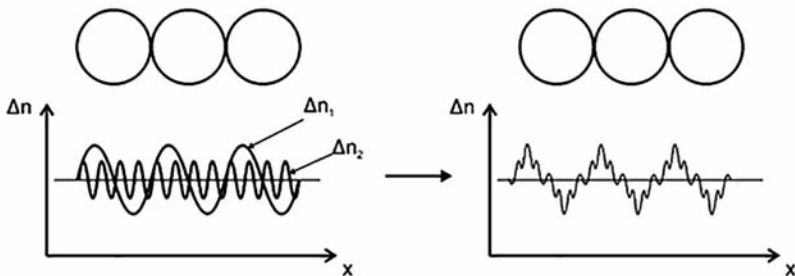

Fig. 1. To the analysis of model representations (object A)
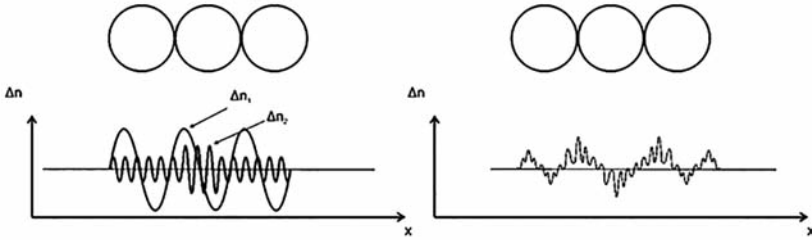
Fig. 2. To the analysis of model representations (object — type B)

Taking into deviation (4) and (5), polarization azimuth maps are determined for the next spatial-frequency filtering

$$\begin{cases} \hat{\alpha}(\kappa,\gamma) = \\ = 0,5\,\mathrm{arctg}\left(\dfrac{\hat{E}_x\hat{E}_y^* - \hat{E}_y\hat{E}_x^*}{\hat{E}_x\hat{E}_x^* - \hat{E}_y\hat{E}_y^*}\right) \\ \dot{\alpha}(\psi) = \\ = 0,5\,\mathrm{arctg}\left(\dfrac{\dot{E}_x\dot{E}_y^* - \dot{E}_y\dot{E}_x^*}{\dot{E}_x\dot{E}_x^* - \dot{E}_y\dot{E}_y^*}\right) \end{cases} \quad (6)$$

Results

We use two types of model polymer objects:

1. Object 1 (A) — it is a network of ordered circular cylinders with two-frequency harmoniously components (low-frequency component $\Delta n_1 = \Delta n_0 \mathrm{Sin}\left(\dfrac{2\pi}{4X_0}x\right)$ and high-frequency component $\Delta n_2 = \Delta n_0^* \mathrm{Sin}\left(\dfrac{2\pi}{X_0}x\right)$) linear anisotropy (fig. 1);

2. Object 2 (B) — it's a similar network, where the central five cylinders are characterized by an increased level (up to 3 times) of the linear birefringence Δn_0^* (fig. 2).

On fig. 3 shows the coordinate distributions of the maps of azimuth of polarization of the Fourier spectrum of the type A network (a) and the spatially-frequency filtered distribution of the maps of azimuth (b).
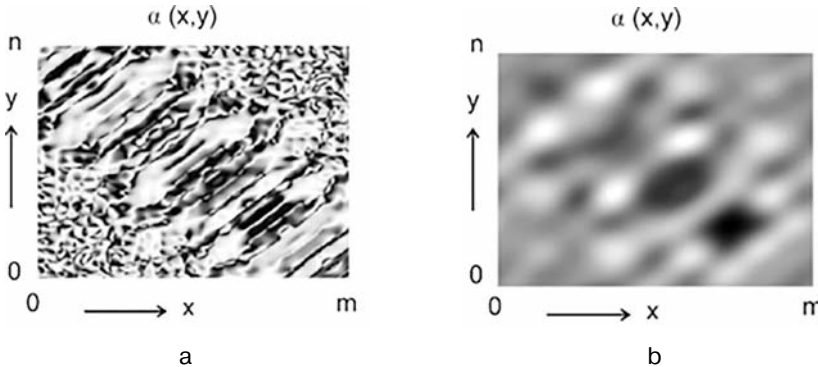
a   b

Fig. 3. Coordinate distributions (a) and large-scale (b) component
of the azimuth of polarization (type A)

On fig. 4 are shown the spatially-frequency filtered distributions of the azimuths maps of the large-scale component of the polycrystalline polymer network with linear birefringence (a) and their statistical characteristics (b).

Comparative characteristics of polarization azimuth maps are illustrated in table 1.

Table 1

Statistical moments of a large-scale polarization map of the azimuth

Parameters	LS (large-scale)	
	A-type	B-type
M_1	0.29	0.33
M_1	0.23	0.27
M_1	0.83	1.69
M_1	1.13	3.47

Discussion

On fig. 5 shows the coordinate distributions of the azimuth maps of a model object (type A) before and after using spatial-frequency filtering with a high-frequency $\Delta R^{-1} = 60$ pixels (size of filter).

The data obtained demonstrate the possibility of using a high-frequency filter, which makes it possible to effectively extract the small-scale component of the coordinate distribution of azimuths by using the inverse Fourier transform.

The results of statistical analysis are presented in fig. 6 and in table 2.

Table 2

Statistical moments of a small-scale map of the azimuth

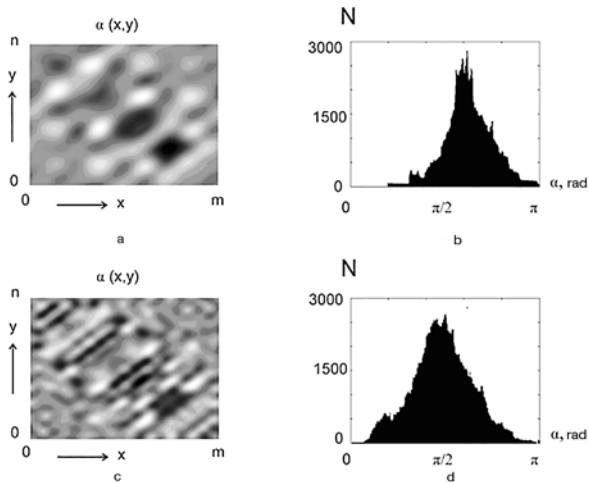| Parameters	HF (small-scale)	
	A-type	B-type
M_1	0.074	0.087
M_1	0.12	0.14
M_1	0.56	0.81
M_1	2.06	0.58

Fig. 4. Large-scale map (a, c) and histogram (b, d) of the coordinate distribution of the maps of azimuth (A-type of polycrystalline network)
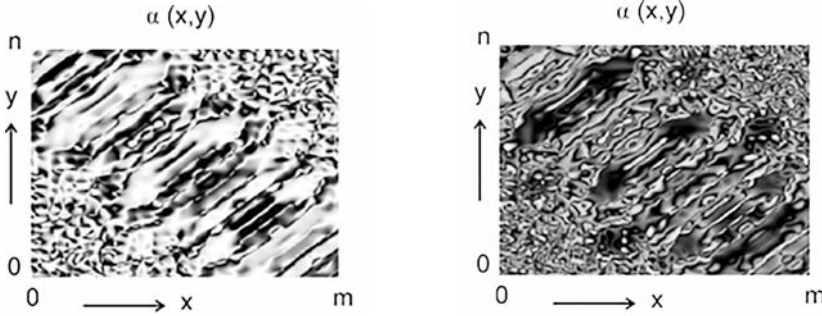
Fig. 5. Coordinate distribution (m*n) and their small-scale component of the azimuth maps of both types (A and B networks)

Comparison of the parameters that characterize the coordinate distributions of the polarization azimuth showed the following main changes in the high-frequency component of linear birefringence.

Firstly, this is a significant expansion of the values, as well as an increase in the histogram scatter of the small-scale component of the polarization azimuth $\alpha(x, y)$ maps, which is formed by the B-type model grid.

Secondly, an increase in the depth of modulation of the high-frequen- cy component of linear birefringence manifests itself in the formation of an inhomogeneous distribution $\alpha(x, y)$.

Conclusions

Comparison of the obtained results of spatial-frequency filtering of the distributions of polarization azimuths of model objects revealed the following parameters, which are diagnostically sensitive to changes in birefringence:

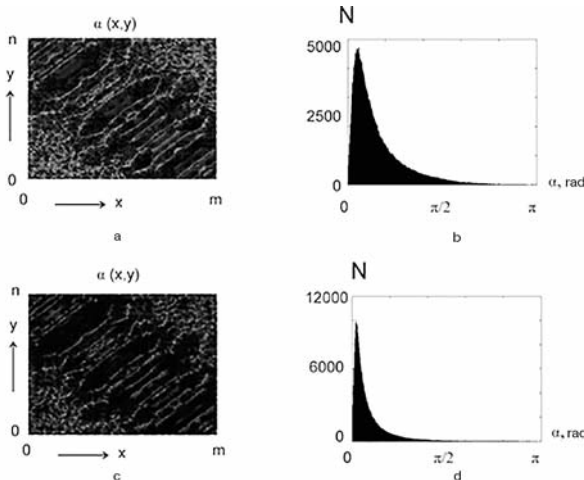— statistical moments of the 3rd and 4th order of orders. The differ-

Fig. 6. Small-scale maps (a, c) and histograms (b, d) of the azimuth distributions of a polycrystalline networks (A-type and B-type)

ences between the values of this data of both types range from 2 (M_3) to 3.5 (M_4) times;

— statistical moments of the 2nd–4th orders of the azimuth distribu-tions and small-scale component of the polarization map of the image of a grid of optically bnirefringence cylinders. The differences from 1.5 (M_2, M_3) to 4 (M_4) times.

References

1. Kim, Dah Hee, & Song, Young Seok (2015). Anisotropic optical film em-bedded with cellulose nanowhisker. *Carbohydrate Polymers*, Vol. 130, 448–454.

2. Roeder, M., Schilling, P., Hera, D., Guenther, T., Z& Zimmermann, A. (2018). Influences on the Fabrication of Diffractive Optical Elements by Injection Com-pression Molding. *J. Manuf. Mater. Process*, 2(1), 5.

3. Doushkina, V. (2010). Advantages of Polymer and Hybrid Glass-Polymer Optics. *Photonics Spectra*, 44(4), 54–58.

4. Schmitt, R., Mallmann, G., Devrient, M., & Schmidt, M. (2014). 3D Poly-mer Weld Seam Characterization Based on Optical Coherence Tomography for Laser Transmission Welding Applications. *Physics Procedia*, Vol. 56, 1305–1314.

5. Ushenko, A. G., Misevich, I. Z., Istratiy, V., Bachyns'ka, I., Peresunko, A. P., Numan, O. K., & Moiysuk, T. G. (2010). Evolution of statistic moments of 2D-dis-tributions of biological liquid crystal netmueller matrix elements in the process of their birefringent structure changes. *Advances in Optical Technologies*. ID 423145.

6. Yermolenko, S., Ushenko, A., Ivashko, P., Goudail, F., Gruia, I., Gavrilă, C., Zimnyakov, D., & Mikhailova, A. (2009). Spectropolarimetry of cancer change of biotissues. *Proceedings of SPIE*, Vol. 7388, 73881D.

7. Angelsky, O. V., Ushenko, A. G., Ushenko, Yu. A., & Ushenko, Ye. G. (2006). Polarization singularities of the object field of skin surface. *J. Phys. D: Appl. Phys*, Vol. 39, 3547–3558.

8. Wang, Mingchuan, Zhang, Kai, & Chen, Cai (2022). A mixed FFT-Galerkin approach for incompressible or slightly compressible hyperelastic solids under finite deformation. *Computer Methods in Applied Mechanics and Engineering*, Vol. 396, 115092.

9. Devlaminck, Vincent, Terrier, Patrick, & Charbois, Jean-Michel (2013). Differential matrix physically admissible for depolarizing media: the case of diagonal matrices. *Opt. Lett.*, 38, 1497–1499.

10. Ossikovski, Razvigor, Anastasiadou, Makrina, & De Martino, Antonello (2008). Product decompositions of depolarizing Mueller matrices with negative determinants. *Optics Communications*, Vol. 281, Issue 9, 2406–2410.

В роботі запропоновано використання лазерно-поляри-метричного методу, який є більш інформативний в сенсі відображення оптично неоднорідних структур за рахунок використання просторово-когерентної фільтрації.

Ключові слова: прикладне програмування; полімери; пакувальна продукція; цифрова та графічна інформація; матеріалознавство.